The Crab Nebula and Mkn 421 High-Energy Gamma-Ray Spectra from CELESTE Observations in 1999-2000

F. Piron, J. Lavalle, A. Jacholkowska and J. Bussons Gordo
Groupe d'Astroparticules de Montpellier, CC 085 Univ. de Montpellier II
Place E. Bataillon, 34095 Montpellier Cedex 5, France (email: piron@in2p3.fr)
for the CELESTE collaboration

Abstract

This is the first report on spectral measurements from 50 GeV for the Crab nebula and from 70 GeV for the blazar Markarian 421. Both sources were detected by the CELESTE experiment in 1999-2000. Here we present the energy measurement and spectral reconstruction methods. The energy resolution is shown to smoothly vary with energy, with a mean value of ∼20% above the detection threshold. Preliminary spectra are presented and compared with those obtained quasi-simultaneously above 300 GeV by the CAT imaging telescope.

1. Introduction

The energy window around 50 GeV was opened by the CELESTE experiment during the winter 1999-2000 with the detection of the Crab nebula and its flux measurement above 60 GeV [2]. Nearly at the same time, CELESTE detected the blazar Markarian 421 (Mkn 421) during a series of flares. It is the first sub-100 GeV atmospheric Cherenkov detection of Mkn 421, and the emission observed by CELESTE is well correlated with the flux above 300 GeV recorded by the CAT telescope, operating on the same site [3]. More recently, the STACEE experiment studied the variability of the Mkn 421 flux above 140 GeV during its 2001 outburst [1]. A correlation was found with the flux recorded by the Whipple imaging telescope (> 390 GeV) and by the RXTE/ASM detector ($2-12$ keV).
Blazars are radio-loud Active Galactic Nuclei with a relativistic jet pointed directly to the observer. The jet emission is variable and dominates that of the accretion disk (and of the host galaxy) over a large energy domain. Thus, blazar observations offer the possibility of investigating the physics of jets more deeply, including particle acceleration and energy extraction in the vicinity of the AGN's central "engine". The high-energy part of the Mkn 421 spectral energy distribution (SED) is generally interpreted as the result of the inverse Compton process involving synchrotron radiation photons and the same relativistic electrons which

pp. 1–8

emitted them. This mechanism, which is also invoked to explain the Crab nebula broad-band SED, predicts that the γ-ray peak energy lies at a few tens of GeV in both cases.
This work covers the first spectral analysis of these sources with CELESTE. The γ-ray energy measurement and the spectral reconstruction are described in Sect. (2.). In Sect. (3.) we present the results and compare them to those obtained by the EGRET and CAT detectors.

2. Energy measurement and spectral reconstruction

2.1. Experimental setup and gamma-ray signal extraction

The experimental setup of CELESTE ("CErenkov Low Energy Sampling and Timing Experiment") is fully described in [6,2]. Briefly, this detector records the Cherenkov light emitted by the secondary particles produced during the development of cosmic-ray atmospheric showers, and was designed to minimize the night-sky noise with a view to achieving a low energy threshold. Until October 2001 it used 40 heliostats (54 m^2 each) of the former solar plant in Thémis, and fast electronics ($\sim$1 GHz flash ADCs) suited to the duration of the Cherenkov signal (a few ns). As explained in [2], good discrimination between γ and charged cosmic-ray induced showers is achieved using the differences between both types of showers regarding the homogeneity and the time distribution of the Cherenkov light pool as sampled by the heliostats. The corresponding event selection is based on the two variables $\sigma_{\rm grp}$, which is the relative RMS of collected charge over the five heliostat groups entering the trigger logic, and θ, the shower axis angle relative to the source direction. A padding procedure and a software trigger are applied to the data to stabilize the background level near the detection threshold and to compensate for changes in the detector response (including the atmosphere) between different observations. The γ-ray signal accrues as the difference in the rate of ON and OFF-source selected events ($\sigma_{\rm grp} < 0.3$ and $\theta^2 < 50\,{\rm mrad}^2$).

2.2. Energy measurement

The energy measurement method has been developped using extensive simulations of the detector for a true γ-ray energy ranging from 30 GeV to 1 TeV. It relies simply on the mean collected charge over the 40 heliostats, $Q_{\rm m}$, and on the measured shower impact parameter, $P_{\rm m}$. The latter corresponds to the maximum emission in the shower core at 11 km and is obtained with an accuracy of 15 m by reconstructing the Cherenkov wave front [2]. For a fixed value of $P_{\rm m}$, $Q_{\rm m}$ scales with the true γ-ray energy: $\log(Q_{\rm m}) = p_1 + p_2 \log(E_{\rm t})$. Thus, we can construct a first variable $E_{\rm m}^{50} = \alpha_1 Q_{\rm m}^{\alpha_2}$, which measures correctly the true

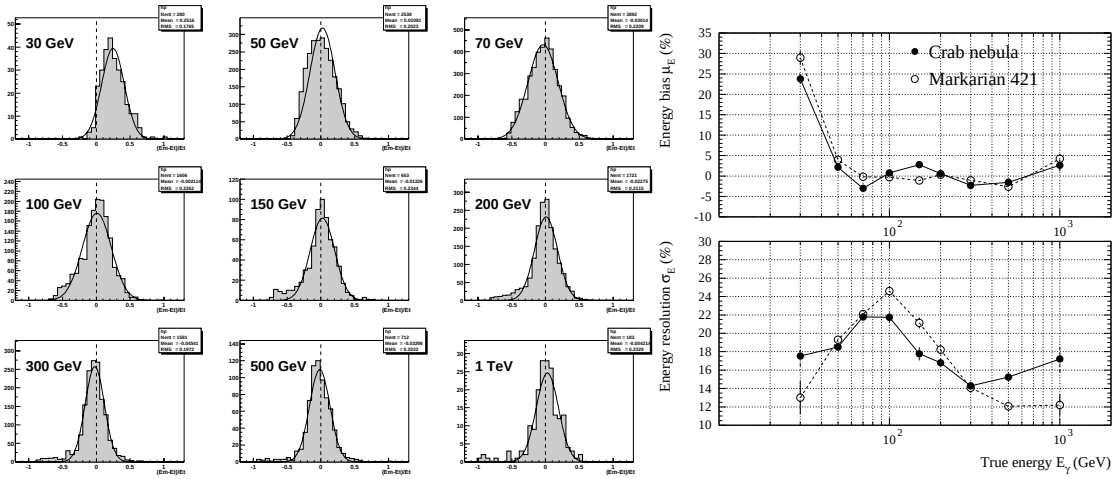

Fig. 1. *(left)* Monte-Carlo energy resolution functions $\mathcal{D}(E_\mathrm{m}/E_\mathrm{t}-1)$ for fixed γ-ray energies between 30 GeV and 1 TeV at Crab transit; *(right)* energy bias $\mu_\mathrm{E} = \overline{E_\mathrm{m}/E_\mathrm{t}-1}$ and energy resolution $\sigma_\mathrm{E} = \sigma(E_\mathrm{m}/E_\mathrm{t}-1)$ as functions of the true energy E_t.

energy if the impact parameter $P_\mathrm{m} = 50$ m. Then the study of the shape of the function $E_\mathrm{m}^{50}/E_\mathrm{t} = f(P_\mathrm{m})$, which is determined by the convolution of the Cherenkov light density on the ground with the detector sampling response, leads to an approximation for intermediate values of P_m : $E_\mathrm{m}^{50}/E_\mathrm{t} \simeq 1 + p_3(P_\mathrm{m}-50)$ for 20 m $< P_\mathrm{m} <$ 80 m. The γ-ray efficiency of this cut lies between 77% and 85%, which is reasonable. The slope p_3 is found to be related to E_t in a simple manner: $p_3 = \alpha_3/E_\mathrm{t} + \alpha_4$. Combining the preceeding equations, one ends up with the following measured energy: $E_\mathrm{m} = \dfrac{\alpha_1 Q_\mathrm{m}^{\alpha_2} - \alpha_3(P_\mathrm{m}-50)}{1+\alpha_4(P_\mathrm{m}-50)}$. The corresponding energy resolution functions $\mathcal{D}(E_\mathrm{m}/E_\mathrm{t}-1)$ are shown in Fig. (1.): they are unbiased above the detection threshold and can be well fitted by centered gaussians with resolutions varying between 12% and 24%.

2.3. Spectral reconstruction

Our method is inspired by the paper by Yost [8] and leads to a three step procedure. First, we choose large energy bins Δ_E^i with respect to the energy resolution σ_E in order to decouple energy resolution effects and acceptance corrections: $E_\mathrm{m} \in [50-100]$, $[100-200]$ and $[200-400]$ GeV. Then, we estimate the *mean true energy* $\widetilde{E}^i \equiv \widetilde{\langle E_\mathrm{t}\rangle}^i$ in each bin by a maximum likelihood fit based on an event-by-event calculation. For each event, the probability density function of measuring E_m is $f(E_\mathrm{m}|E_0) = \displaystyle\int \mathrm{d}E_\mathrm{t}\ (\mathrm{d}\mathcal{P}/\mathrm{d}E_\mathrm{t})\ \frac{1}{\sqrt{2\pi\sigma_\mathrm{E}^2}} \exp\Big[-\frac{(E_\mathrm{m}-E_\mathrm{t})^2}{2\sigma_\mathrm{E}^2}\Big]$. According to

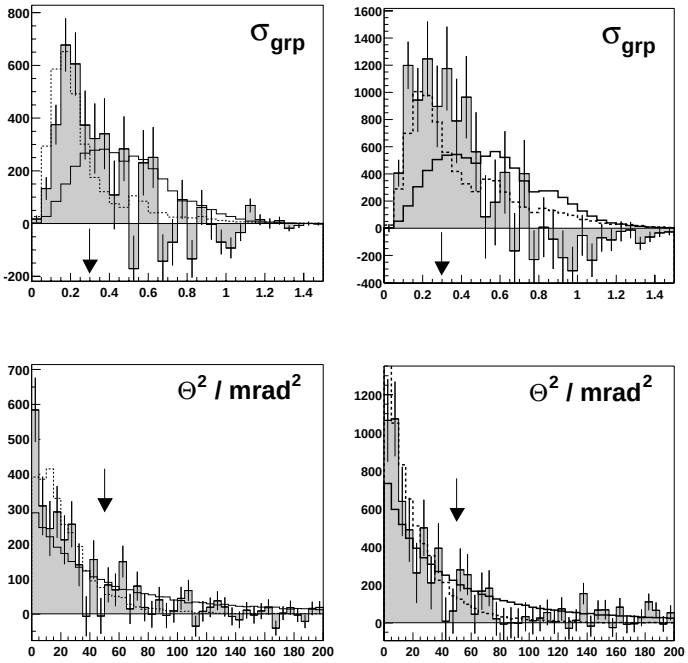

Fig. 2. $\sigma_{\rm grp}$ and θ^2 distributions for ON-OFF data (shaded histogram with error bars), renormalised OFF data (thick solid line) and renormalised γ-ray simulations (thick dashed line) for the Crab nebula sample (left) and for Mkn 421 (right). Arrows show the cuts applied for the γ-ray signal extraction. Note that $\sigma_{\rm grp}$ is the best discriminating variable.

simulations, the normalized distribution of the true energy after acceptance and analysis cuts is exponential above the threshold, $\mathrm{d}\mathcal{P}/\mathrm{d}E_{\rm t} = P_0 \exp(-E_{\rm t}/E_0)$. The maximization of the likelihood function $\mathcal{L}(E_0) = \prod_{\rm events} f(E_{\rm m}|E_0)$ yields the expectation value $\widetilde{E}^i = E_0$. Finally, the differential flux Φ_i at $\widetilde{E}^i$ is computed through $\Phi_i = (N^i_{\rm ON} - N^i_{\rm OFF})/(\Delta^i_{\rm E}\, T_{\rm obs}\, \mathcal{A}_i)$. The weighted acceptance over the bin, $\mathcal{A}_i = \int \mathcal{A}(E)\; E^\gamma \,\mathrm{d}E \;/ \int E^\gamma \,\mathrm{d}E$, depends on the shape of the source spectrum, which is here assumed to follow a power-law $\mathrm{d}N/\mathrm{d}E = \phi_0[E/100\,\mathrm{GeV}]^\gamma$. The spectral index γ is thus determined through an iterative procedure. Note that the overall method has been validated using simulated spectra generated with different indexes.

3. Results

3.1. Data samples

A data selection requiring good weather conditions and stable detector operation has been applied. Moreover, we restrict the analysis to the data taken near transit in order to avoid large acceptance variations. This leaves $T_{\rm obs} = 3.5\,$h of ON-source data for the Crab nebula within 1h from transit (in single pointing mode), and $T_{\rm obs} = 22.1\,$h for Mkn 421 mostly within 1-2h from transit (in single and double pointing mode, see [2] for details). Since Mkn 421 data were taken further from transit, a dedicated simulation was needed to estimate the γ-ray acceptance $\mathcal{A}(E)$ and to check that the energy measurement method is still valid

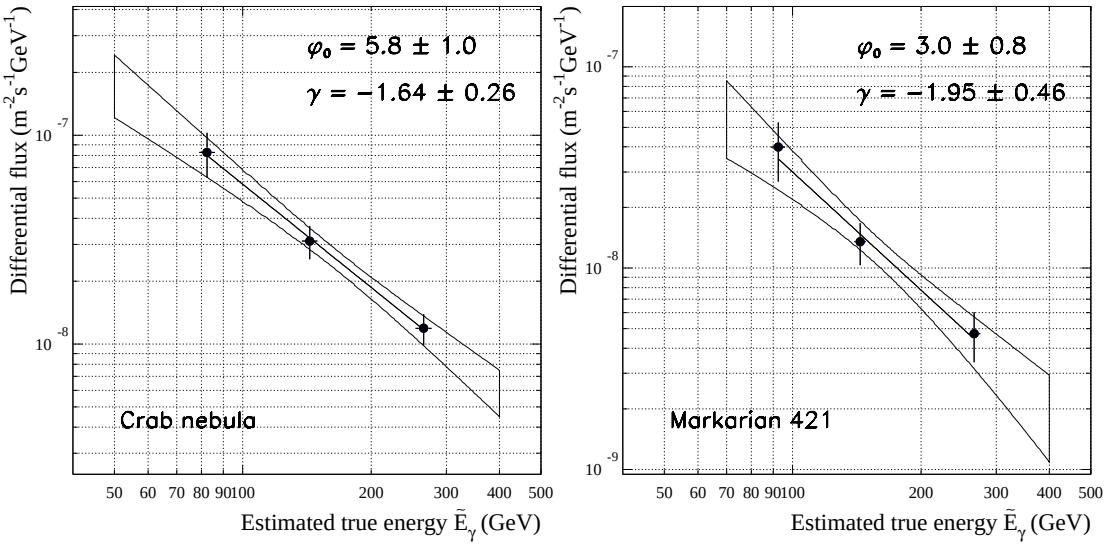

Fig. 3. Differential spectrum of the Crab nebula (left) and Mkn 421 (right), for an assumed power-law shape $\mathrm{d}N/\mathrm{d}E = \phi_0[E/100\,\mathrm{GeV}]^{\gamma}$. The flux constant ϕ_0 is given in units of $10^{-8}\,\mathrm{m}^{-2}\,\mathrm{s}^{-1}\,\mathrm{GeV}^{-1}$, and the outer box shows the 68% confidence level contour, taking account of the correlation between ϕ_0 and γ.

in this region. Moreover, the energy threshold for the elevation range of this source is 70 GeV.

The data samples are shown in Fig. (2.) after the event selection quoted in Sect. (2.1.). When restricting to $20\,\mathrm{m} < P_\mathrm{m} < 80\,\mathrm{m}$, we observe 1411 ± 169 γ-rays between 50 GeV and 400 GeV for the Crab nebula and 3277 ± 427 γ-rays between 70 GeV and 400 GeV for Mkn 421.

3.2. Spectra

The differential spectra are shown in Fig. (3.). Systematic errors (not shown on this plot) arise from the method explained in Sect. (2.) and from the absolute energy scale uncertainty, which is largely dominant*: assuming, like in [2], an absolute uncertainty of 30% on E_m, one gets $\Delta\phi_0/\phi_0 \simeq \pm 20\%$ and $\Delta\gamma \simeq (^{+0.10}_{-0.62})$. The broad-band SEDs are shown in Fig. (4.): the proper combination of statistical and systematic errors leads to an asymmetric 68% confidence level contour. These preliminary results are compatible with the contemporary measurements above 300 GeV from the CAT telescope and, for the Crab nebula, with the flux published by CELESTE in [2]. They confirm that CELESTE is well suited to study the γ-ray peak of both sources.

*Note that the errors on acceptance and cuts efficiencies are assumed here to be negligible, despite slight discrepancies shown in Fig. (2.) between ON-OFF data and γ-ray simulations.

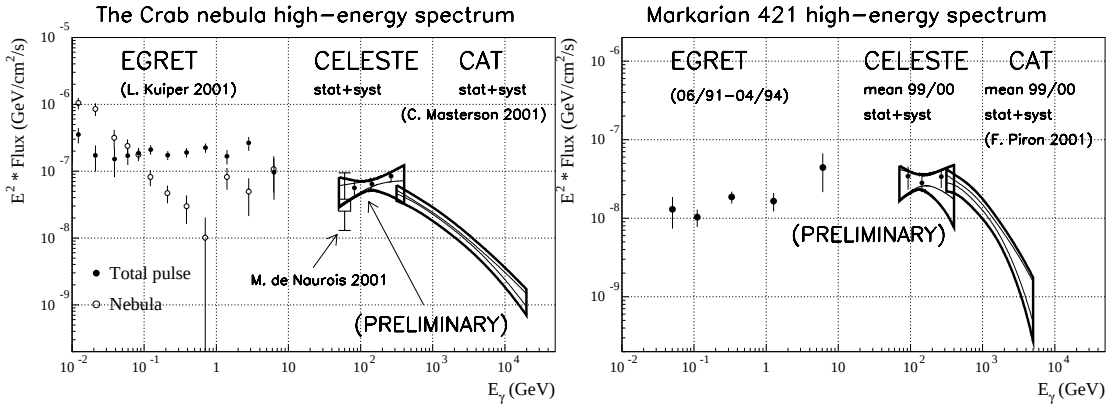

Fig. 4. The Crab nebula (left) and Mkn 421 (right) broad-band SEDs as measured by CGRO/EGRET, CELESTE ([2] and this work) and CAT. For ground-based experiments, the inner thin contours stand for statistical errors only, while the outer thick contours combine statistical and systematic errors.

4. Conclusions

This work reports the first spectral analysis performed by CELESTE. Using a simple algorithm, an energy resolution of ∼20% can be achieved. The spectra of the Crab nebula and of Mkn 421 have been measured with 40 active heliostats above an energy threshold of 50 GeV and 70 GeV, respectively. These preliminary spectra are compatible with contemporary results from the CAT telescope above 300 GeV. Future work will include the extension of the data set to larger zenith angles. However, systematic errors remain still large and their study will continue. In particular, the LIDAR data regularly taken on the Thémis site since January 2002 are under analysis and should allow reduction of the systematic uncertainties due to changing atmospheric conditions during observations.

5. References

1. Boone L.M. et al. 2002, ApJL 579, 5
2. de Naurois M. et al. 2002, ApJ 566, 343
3. Holder J. 2001, in "High-Energy Gamma-Ray Astronomy" (Heidelberg), AIP Conf. Proc. 558, ed. F. A. Aharonian & H. J. Voelk, 635
4. Kuiper L. et al. 2001, A&A 378, 918
5. Masterson C. 2001, AIP Conf. Proc. 558, 753
6. Paré E. et al. 2002, NIM A490, 71
7. Piron F. et al. 2001, A&A 374, 895
8. Yost G.P. 1984, NIM 234, 489